MIT Open Access Articles

System size dependence of cluster properties from two-particle angular correlations in Cu +Cu and Au+Au collisions at sqrt[s_{NN}]=200 GeV

Massachusetts Institute of Technology

System size dependence of cluster properties from two-particle angular correlations in Cu + Cu and Au + Au collisions at $\sqrt{s_{NN}} = 200$ GeV

B. Alver,[4] B. B. Back,[1] M. D. Baker,[2] M. Ballintijn,[4] D. S. Barton,[2] R. R. Betts,[6] R. Bindel,[7] W. Busza,[4] Z. Chai,[2] V. Chetluru,[6] E. García,[6] T. Gburek,[3] K. Gulbrandsen,[4] J. Hamblen,[8] I. Harnarine,[6] C. Henderson,[4] D. J. Hofman,[6] R. S. Hollis,[6] R. Hołyński,[3] B. Holzman,[2] A. Iordanova,[6] J. L. Kane,[4] P. Kulinich,[4] C. M. Kuo,[5] W. Li,[4,*] W. T. Lin,[5] C. Loizides,[4] S. Manly,[8] A. C. Mignerey,[7] R. Nouicer,[2] A. Olszewski,[3] R. Pak,[2] C. Reed,[4] E. Richardson,[7] C. Roland,[4] G. Roland,[4] J. Sagerer,[6] I. Sedykh,[2] C. E. Smith,[6] M. A. Stankiewicz,[2] P. Steinberg,[2] G. S. F. Stephans,[4] A. Sukhanov,[2] A. Szostak,[2] M. B. Tonjes,[7] A. Trzupek,[3] G. J. van Nieuwenhuizen,[4] S. S. Vaurynovich,[4] R. Verdier,[4] G. I. Veres,[4] P. Walters,[8] E. Wenger,[4] D. Willhelm,[7] F. L. H. Wolfs,[8] B. Wosiek,[3] K. Woźniak,[3] S. Wyngaardt,[2] and B. Wysłouch[4]

[1]*Argonne National Laboratory, Argonne, Illinois 60439-4843, USA*
[2]*Brookhaven National Laboratory, Upton, New York 11973-5000, USA*
[3]*Institute of Nuclear Physics PAN, Kraków, Poland*
[4]*Massachusetts Institute of Technology, Cambridge, Massachusetts 02139-4307, USA*
[5]*National Central University, Chung-Li, Taiwan*
[6]*University of Illinois at Chicago, Chicago, Illinois 60607-7059, USA*
[7]*University of Maryland, College Park, Maryland 20742, USA*
[8]*University of Rochester, Rochester, New York 14627, USA*

We present results on two-particle angular correlations in Cu + Cu and Au + Au collisions at a center-of-mass energy per nucleon pair of 200 GeV over a broad range of pseudorapidity (η) and azimuthal angle (ϕ) values as a function of collision centrality. The PHOBOS detector at the Relativistic Heavy Ion Collider has a uniquely large angular coverage for inclusive charged particles, which allows for the study of correlations on both long- and short-range scales. A complex two-dimensional correlation structure in $\Delta\eta$ and $\Delta\phi$ emerges, which is interpreted in the context of a cluster model. The effective cluster size and decay width are extracted from the two-particle pseudorapidity correlation functions. The effective cluster size found in semicentral Cu + Cu and Au + Au collisions is comparable to that found in proton-proton collisions but a nontrivial decrease in size with increasing centrality is observed. Moreover, a comparison of results from Cu + Cu versus Au + Au collisions shows an interesting scaling of the effective cluster size with the measured fraction of total cross section (which is related to the ratio of the impact parameter to the nuclear radius, $b/2R$), suggesting a geometric origin. Further analysis for pairs from restricted azimuthal regions shows that the effective cluster size at $\Delta\phi \sim 180°$ drops more rapidly toward central collisions than the size at $\Delta\phi \sim 0°$. The effect of limited η acceptance on the cluster parameters is also addressed, and a correction is applied to present cluster parameters for full η coverage, leading to much larger effective cluster sizes and widths than previously noted in the literature. These results should provide insight into the hot and dense medium created in heavy ion collisions.

I. INTRODUCTION

Multiparticle correlation studies have played an important role in exploring the underlying mechanism of particle production in high-energy hadronic collisions. In $p + p$ collisions, inclusive two-particle correlations have been found to have two components: "intrinsic" two-particle correlations as well as an effective "long-range" correlation owing to event-by-event fluctuations of the overall particle multiplicity (see, e.g., Ref. [1]). By considering the two-particle rapidity density at fixed multiplicity, the intrinsic correlations between particles were isolated and found to be approximately Gaussian, with a range of $\sigma_\eta \sim 1$ unit in pseudorapidity $\{\eta = -\ln[\tan(\theta/2)]\}$. These correlations have conventionally been called "short range." Their properties have been characterized by the concept of "cluster emission" [2].

The simple idea that hadrons are produced in clusters, rather than individually, has had great success in describing many features of particle production [1–4]. In this scenario, hadronization proceeds via "clusters," high-mass states (e.g., resonances but not necessarily with all well-defined quantum numbers) that decay isotropically in their rest frame into the final-state hadrons. An independent cluster emission model (ICM) has been widely applied to the study of two-particle correlations [1–5], where clusters are formed before the final-state hadrons and are independently emitted according to a dynamically generated distribution in η and ϕ. The clusters subsequently decay isotropically in their own rest frame into the observed final-state hadrons. The observed correlation strength and extent in phase space can be parameterized in terms of the cluster multiplicity, or "size" (the average number of particles in a cluster), and the decay "width" (which characterizes the separation of the particles in pseudorapidity). However, it should be noted that independent cluster emission is only a phenomenological approach and provides no insight

_____
*davidlw@mit.edu

into the mechanisms by which clusters are formed. Further modeling is required to connect these studies to the underlying QCD dynamics.

Measurement of cluster properties from two-particle correlations in $p + p$ collisions for particles emitted into $|\eta| < 3$ was performed previously at center-of-mass energies ($\sqrt{s}$) of 200 and 410 GeV using the PHOBOS detector at the Relativistic Heavy Ion Collider (RHIC) [6]. The data suggested an effective cluster size (K_{eff}; defined in Sec. IV) of 2.44 ± 0.08 at $\sqrt{s} = 200$ GeV, increasing with collision energy and event multiplicity. The results are consistent with previous measurements from ISR and S$p\bar{p}$S at various energies [1,3,4].

In heavy ion collisions at RHIC, it has been predicted that the formation of a strongly interacting quark gluon plasma could modify cluster properties relative to $p + p$ collisions [7]. In order to systematically explore the properties of the clusters from $p + p$ to $A + A$ collisions, this paper presents the results on two-particle angular correlations in Cu + Cu and Au + Au collisions at a center-of-mass energy per nucleon pair ($\sqrt{s_{NN}}$) of 200 GeV, over a very broad acceptance in $\Delta\eta\ (=\eta_1 - \eta_2)$ and $\Delta\phi\ (=\phi_1 - \phi_2)$. The PHOBOS Octagon detector, covering pseudorapidities of $-3 < \eta < 3$ over almost the full azimuth, is well suited to measure the correlations between particles emitted from clusters. The two-dimensional (2D) correlation functions in Cu + Cu and Au + Au collisions, as well as the extracted effective cluster size and width from one-dimensional (1D) $\Delta\eta$ correlation functions, are presented as a function of system size. By separating particle pairs into "near side" ($0° < \Delta\phi < 90°$) and "away side" ($90° < \Delta\phi < 180°$), more detailed information on the properties of the clusters is obtained. Furthermore, by extrapolating limited acceptance ($|\eta| < 3$) to full phase space, cluster properties unbiased by detector acceptance have been estimated. This comprehensive analysis of cluster properties in $p + p$ and $A + A$ collisions should provide useful information for understanding the hadronization stage but may also give insight into physics relevant at much earlier times.

II. DATA SETS

The data presented here for Cu + Cu and Au + Au collisions at $\sqrt{s_{NN}} = 200$ GeV were collected during RHIC Run 4 (2004) and Run 5 (2005) using the large-acceptance PHOBOS Octagon silicon array covering pseudorapidity $-3 < \eta < 3$ over almost the full azimuth. A full description of the PHOBOS detector is given in Ref. [8]. The primary event trigger used the time difference between signals in two sets of 10 Cerenkov counters, located at $4.4 < |\eta| < 4.9$, to select collisions that were close to the nominal vertex position $z_{vtx} = 0$ along the beam axis. About 4 million events each of Cu + Cu and Au + Au collisions at $\sqrt{s_{NN}} = 200$ GeV were selected for further analysis by requiring that the primary collision vertex falls within $|z_{vtx}| < 6$ cm.

The angular coordinates (η, ϕ) of charged particles are measured using the location of the energy deposited in the silicon pads of the Octagon. The granularity of the Octagon is determined by the sizes of the readout pads, which are about $11.25°\ (\sim 0.2$ rad) in ϕ and range from 0.006 to 0.05 in η. Noise

and background hits are rejected by placing a lower threshold on the deposited energy corrected for the path length through the silicon after hit merging, assuming that the charged particle originated from the primary vertex. Depending on η, merged hits with less than 50%–60% of the energy loss expected for a minimum ionizing particle are rejected. More details of the hit reconstruction procedure are given in Ref. [9].

III. ANALYSIS PROCEDURE

The detailed analysis procedure is described in Ref. [6]. The inclusive two-particle correlation function in $(\Delta\eta, \Delta\phi)$ space is defined as follows:

$$
\begin{aligned}
R(\Delta\eta, \Delta\phi) &= \left\langle (n-1)\left[\frac{\rho^{\mathrm{II}}(\Delta\eta, \Delta\phi)}{\rho^{\mathrm{mixed}}(\Delta\eta, \Delta\phi)} - 1 \right] \right\rangle \\
&= \frac{\langle (n-1)\rho^{\mathrm{II}}(\Delta\eta, \Delta\phi)\rangle}{\rho^{\mathrm{mixed}}(\Delta\eta, \Delta\phi)} - \langle n-1 \rangle. \quad (1)
\end{aligned}
$$

The first line of Eq. (1) shows the behavior of the correlation function, while its mathematically equivalent second line corresponds to the analysis procedure described later. For a given centrality bin, $\rho^{\mathrm{II}}(\Delta\eta, \Delta\phi)$ (normalized to unit integral) is the foreground pair distribution evaluated event by event by taking pairs within the same event. It is then weighted by a factor, $(n - 1)$ [where n is the total number of hits in each event; generator-level tracks are used in the Monte Carlo (MC) method], and averaged over all the events. The event multiplicity normalization factor, $(n - 1)$, is introduced to compensate for the trivial dilution effects from uncorrelated particles, as the number of uncorrelated pairs grows quadratically with n, whereas the number of correlated pairs grows only linearly. Therefore, $R(\Delta\eta, \Delta\phi)$ is defined in such a way that if a heavy ion collision is simply a superposition of individual $p + p$ collisions, the same correlation function will be observed in both $A + A$ and $p + p$ collisions.

The mixed-event background distribution $\rho^{\mathrm{mixed}}(\Delta\eta, \Delta\phi)$ (also normalized to unit integral) is constructed by randomly selecting two particles from two different events with a similar vertex (with a bin width of 0.2 cm) and centrality (in bins of 5% of the total inelastic cross section), representing a product of two single-particle distributions. Because the background is found to be roughly multiplicity independent within a centrality bin, the inclusive $\rho^{\mathrm{mixed}}(\Delta\eta, \Delta\phi)$ is used in our calculations of Eq. (1) for each centrality class. Thus it can be either inside or outside the event average, as shown in the two lines of Eq. (1). $R(\Delta\eta, \Delta\phi)$ is symmetrized at $\Delta\eta = 0$ and $\Delta\phi = 0$ following the same convention as in the previous publication [6]. As can be inferred from the first line of Eq. (1), because both $\rho^{\mathrm{II}}(\Delta\eta, \Delta\phi)$ and $\rho^{\mathrm{mixed}}(\Delta\eta, \Delta\phi)$ are normalized to unit integral, $R(\Delta\eta, \Delta\phi)$ will range from positive to negative. Therefore, there is no particular significance when $R(\Delta\eta, \Delta\phi) = 0$ in a small region of $\Delta\eta$ and $\Delta\phi$, although $R(\Delta\eta, \Delta\phi) = 0$ everywhere would indicate the absence of correlations.

Corrections for secondary effects and incomplete acceptance have been applied in a similar way to those in $p + p$ collisions, resulting in corrections with comparable
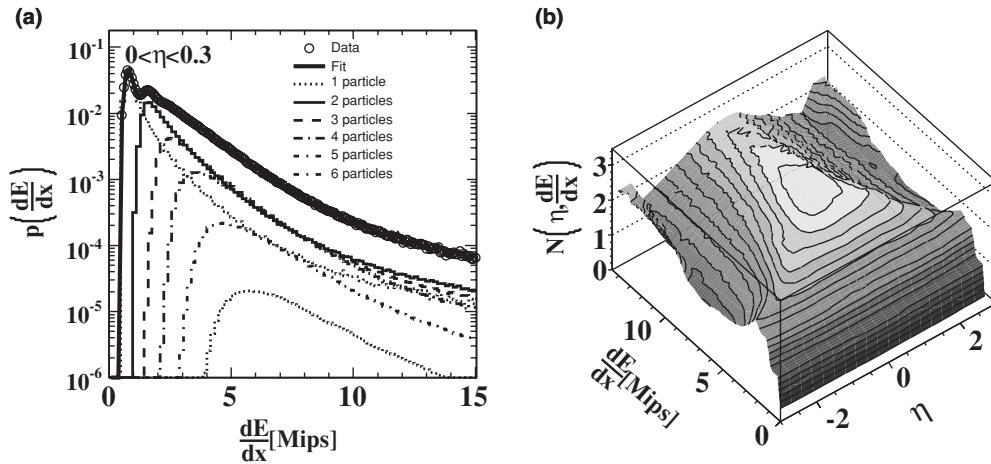
FIG. 1. (a) dE/dx distribution for hits registered in the Octagon in the $0 < \eta < 0.3$ range (open circles) fitted by a sum (solid line) of predicted dE/dx distributions for various numbers of particles hitting a single pad (dashed lines) for the most central 3% of 200-GeV Au + Au collisions. A Mip is defined as the energy deposited by a single minimum-ionizing particle at normal incidence. (b) Estimated average number of particles per silicon pad as a function of η and dE/dx for the most central 3% of 200-GeV Au + Au collisions.

magnitudes [6]. Because the PHOBOS Octagon is a single-layer silicon detector, there is no p_T, charge, or mass information available for the particles. All charged particles above a low-p_T cutoff of about 7 MeV/c at $\eta = 3$, and 35 MeV/c at $\eta = 0$ (which is the threshold below which a charged particle is stopped by the beryllium beam pipe), are included on equal footing. Thus secondary effects, such as δ electrons, γ conversions, and weak decays, cannot all be rejected directly. The incomplete azimuthal acceptance in some pseudorapidity regions naturally suppresses the overall correlation strength, but MC simulations show that it does not change the shape of the correlation function $R(\Delta\eta, \Delta\phi)$. To correct for these detector effects in the data, correlation functions are calculated for MC events (PYTHIA for $p + p$ collisions and HIJING for $A + A$ collisions) at $\sqrt{s} = 200$ GeV both at the generator level for true primary charged hadrons, $R_{\mathrm{pri}}^{\mathrm{MC}}(\Delta\eta, \Delta\phi)$, and with the full GEANT detector simulation and reconstruction procedure, $R_{\mathrm{sim}}^{\mathrm{MC}}(\Delta\eta, \Delta\phi)$. The whole correction procedure can be summarized by the following equation:

$$R_{\mathrm{final}}^{\mathrm{data}}(\Delta\eta, \Delta\phi) = A \times \left[R_{\mathrm{raw}}^{\mathrm{data}}(\Delta\eta, \Delta\phi) - S(\Delta\eta, \Delta\phi) \right], \quad (2)$$

where the function

$$S(\Delta\eta, \Delta\phi) = R_{\mathrm{sim}}^{\mathrm{MC}}(\Delta\eta, \Delta\phi) - R_{\mathrm{pri,acc}}^{\mathrm{MC}}(\Delta\eta, \Delta\phi) \quad (3)$$

represents the correction for secondary effects, which mainly contribute to a large, narrow spike in $R(\Delta\eta, \Delta\phi)$ around $\Delta\eta = 0$, $\Delta\phi = 0$ (for more details, see Ref. [6]). The acceptance correction factor, A, is estimated to be around 1.3, with little dependence on vertex and centrality. The total systematic uncertainty for these corrections is typically about 5% of the final value of $R(\Delta\eta, \Delta\phi)$.

In addition to these corrections, the high occupancies measured in $A + A$ collisions (which are in the range of 50%–60% at midrapidity for the most central 3% of 200-GeV Au + Au collisions) require us to account for the high probability of multiple particles hitting a single pad. The dE/dx distribution

of hits in a very low-multiplicity environment (e.g., 55%–60% peripheral Cu + Cu, which has an occupancy of about 4% at midrapidity) has been measured first in a narrow η bin of 0.3 unit [same bin size as for $R(\Delta\eta, \Delta\phi)$], to approximate the dE/dx distribution for a single particle hitting a single silicon pad, $p_1(dE/dx)$. By convoluting $p_1(dE/dx)$ i times, the dE/dx distribution of i particles hitting a single pad can be predicted: $p_i(dE/dx)$ ($i = 1, 2, 3, \ldots$). Then the dE/dx distribution in more central data events, $p(dE/dx)$, is fitted by a sum of $p_i(dE/dx)$ with weighting factor w_i such that the relative contribution of different numbers of particles hitting on a single pad can be estimated, as illustrated in Fig. 1(a) for the most central 3% of 200-GeV Au + Au collisions as an example. Although the w_i are free parameters in these fits, they have been compared to a Poisson distribution and found to be in very good agreement. The average number of particles per pad can thus be calculated as a function of dE/dx:

$$N\left(\frac{dE}{dx}\right) = \frac{\sum_i i \times w_i \, p_i \left(\frac{dE}{dx}\right)}{\sum_i w_i \, p_i \left(\frac{dE}{dx}\right)}. \quad (4)$$

Performing the procedure above in each η and centrality bin, the average number of particles per pad as a function of dE/dx and η, $N(\eta, dE/dx)$, is derived and shown in Fig. 1(b) for the most central 3% of 200-GeV Au + Au collisions. In calculating the correlation function, each hit is assigned a weight $N(\eta, dE/dx)$ based on its η and dE/dx. Using this procedure, the effects of high occupancy are compensated at the hit level. The systematic uncertainty of the occupancy correction is about 5%–7% ranging from peripheral to central collisions. The effect of occupancy fluctuations within a particular centrality bin has also been investigated. The analysis was repeated both for a much narrower range in multiplicity in the same bin and using the correction weights for a higher-multiplicity bin, and the impact on the final results was found to be negligible.
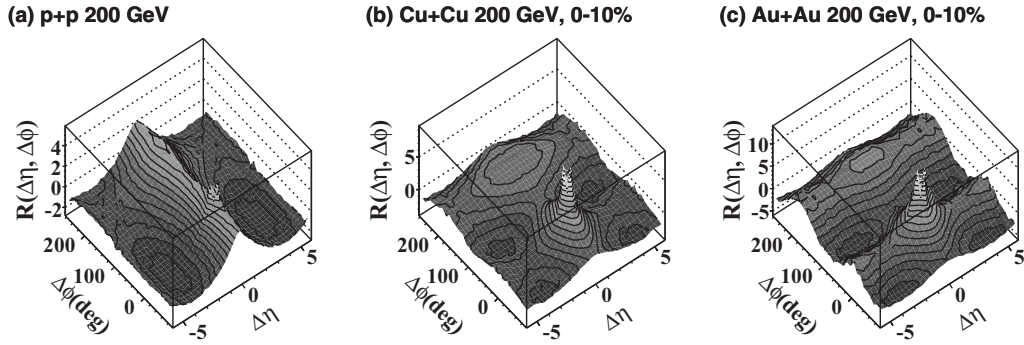
FIG. 2. Two-particle angular correlation functions in $\Delta\eta$ and $\Delta\phi$ for (a) $p + p$, the most central 10% (b) $Cu + Cu$ and (c) $Au + Au$ collisions at $\sqrt{s}$ or $\sqrt{s_{NN}} = 200$ GeV.

IV. RESULTS

The final 2D two-particle inclusive correlation functions for charged particles after all corrections are shown in Fig. 2 as a function of $\Delta\eta$ and $\Delta\phi$ for the most central 10% $Cu + Cu$ (b) and $Au + Au$ (c) collisions at $\sqrt{s_{NN}} = 200$ GeV. For comparison, the previous measurement in $p + p$ collisions [Fig. 2(a)] at the same energy [6] is also shown. In $p + p$ collisions, the complex 2D correlation structure is approximately Gaussian in $\Delta\eta$ and persists over the full $\Delta\phi$ range, becoming broader toward larger $\Delta\phi$. This feature can be qualitatively described by an independent cluster approach, as will be shown later. Compared to $p + p$ collisions, heavy ion collisions show not only the cluster-like structure, but also a $\cos(2\Delta\phi)$ modulation due to elliptic flow [10].

As was done in the analysis of $p + p$ collisions [6], the 2D correlation functions in $A + A$ are integrated over $\Delta\phi$ to give the 1D correlation functions $R(\Delta\eta)$, shown in Fig. 3. This allows a quantitative study of cluster properties in pseudorapidity space, with the elliptic flow contribution

averaging to zero. $R(\Delta\eta)$ is then fitted to a functional form derived in Ref. [5] in an ICM:

$$R(\Delta\eta) = \alpha \left[\frac{\Gamma(\Delta\eta)}{\rho^{\text{mixed}}(\Delta\eta)} - 1 \right], \qquad (5)$$

where $\rho^{\text{mixed}}(\Delta\eta)$ is the background distribution obtained by event mixing and averaged over $\Delta\phi$. The parameter α is equal to $K_{\text{eff}} - 1$, where K_{eff} is the effective cluster size, defined as

$$K_{\text{eff}} = \alpha + 1 = \langle K \rangle + \frac{\sigma_K^2}{\langle K \rangle}, \qquad (6)$$

which depends on the first two moments (mean and σ) of the distribution of cluster size K (number of particles decayed from a cluster) over all clusters in all events. The function $\Gamma(\Delta\eta)$ is a normalized Gaussian function $(1/\sqrt{4\pi}\delta)\exp - [(\Delta\eta)^2/(4\delta^2)]$, where the δ parameter is equal to the width of the $\Delta\eta$ distribution of the particle pairs from a single cluster. It is connected with another variable also characterizing the cluster width, σ_η (understood as the width of the
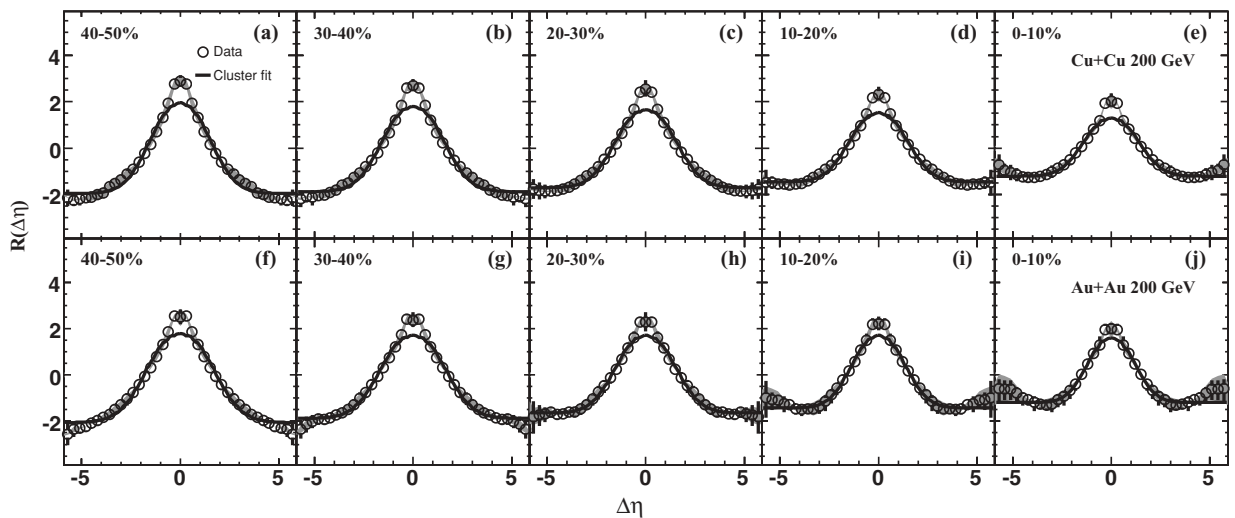

FIG. 3. Two-particle pseudorapidity correlation functions, averaged over the $\Delta\phi$ range from 0° to 180°, in $Cu + Cu$ (upper row) and $Au + Au$ (lower row) collisions for five different centrality classes at $\sqrt{s_{NN}} = 200$ GeV. Solid curves (black) correspond to Eq. (5) with the final values of the parameters (see text for discussion). Error bars and bands (gray) correspond to point-to-point systematic errors and overall scale errors, respectively, with 90% confidence limits. The statistical errors are negligible.

distribution of the difference $\eta_{particle} - \eta_{cluster}$), by the formula, $\delta = \sqrt{K/(K-1)} \times \sigma_\eta$, for fixed K. The factor $\sqrt{K/(K-1)}$ difference is due to the fact that the average of $\eta_{particle}$ in a cluster is constrained to be conserved (equal to $\eta_{cluster}$). Of course, without direct knowledge of the distribution of K, the average cluster size $\langle K \rangle$ and width σ_η cannot be derived based on K_{eff} and δ.

Correlation functions for bins in vertex and centrality are individually fit using Eq. (5) to extract the effective cluster size K_{eff} and the cluster decay width δ for each bin. These results are then averaged over the vertex range to find the final results for each centrality. The averaged correlation functions are shown in Fig. 3 along with a line showing Eq. (5) with the final averaged values of the fit parameters. The three most central points (a region of $|\Delta\eta| < 0.45$) in $R(\Delta\eta)$ are excluded from the fits, mainly because of the large uncertainty stemming from residual detector effects.

Results on effective cluster size (K_{eff}) and decay width (δ) as a function of the fractional cross section, $1 - (\sigma/\sigma_0)$, where σ_0 is the total $A + A$ inelastic cross section, are shown in Fig. 4 for Cu + Cu and Au + Au collisions at $\sqrt{s_{NN}} = 200$ GeV.

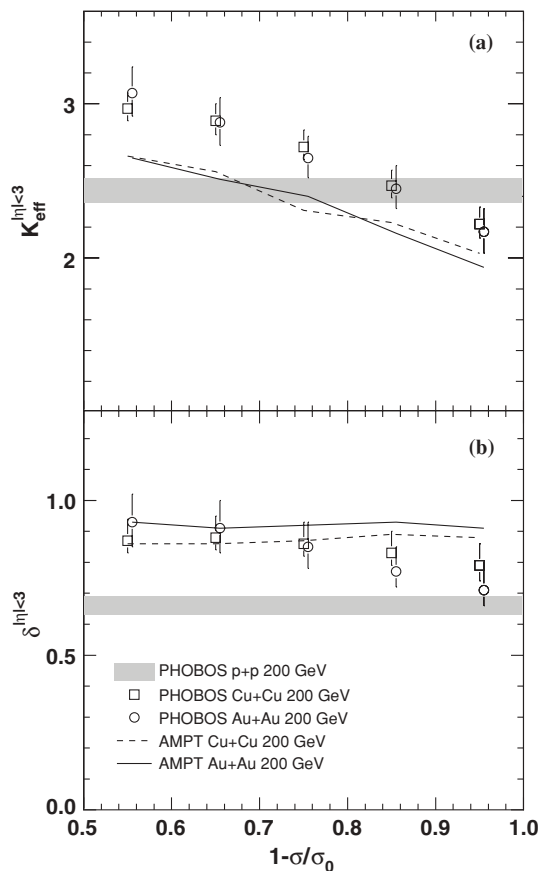FIG. 4. (a) K_{eff} and (b) δ as a function of fractional cross section $[1 - (\sigma/\sigma_0) = 1$ for the most central collisions] for PHOBOS data (open symbols) and for the AMPT model (lines) in Cu + Cu (squares) and Au + Au (circles) collisions for $|\eta| < 3$ at $\sqrt{s_{NN}} = 200$ GeV. Error bars for data points represent systematic errors with 90% confidence limits. Results for $p + p$ collisions at $\sqrt{s} = 200$ GeV [6] are shown by the shaded band.

The systematic uncertainties are estimated using a procedure similar to that for $p + p$ collisions [6], with an additional contribution from the occupancy corrections. The overall scale error, common to both Cu + Cu and Au + Au, is 5% for both K_{eff} and δ. The shaded band in Fig. 4 indicates the value found in $\sqrt{s} = 200$-GeV $p + p$ collisions, which suggests that the cluster properties are similar in $p + p$ and $A + A$ systems. This implies that the phenomenological properties of hadronization are similar in $p + p$ and $A + A$. However, an increase in both the effective cluster size and the decay width is observed upon going from $p + p$ to peripheral $A + A$ systems. Toward more central collisions, it is also observed that the effective cluster size systematically decreases with increasing collision centrality in both Cu + Cu and Au + Au collisions, whereas the cluster decay width is approximately constant over the whole centrality range within the systematic uncertainties. Furthermore, by comparing the two systems at the same fraction of the inelastic cross section (which is related to the ratio of impact parameter b to the radius R of the nucleus, $b/2R$), a "geometric scaling" feature is revealed, which shows a similar effective cluster size at the same collision geometry of the system, that is, the shape of the overlap region. This feature is not obviously expected, as the cluster parameters are constructed to reflect short-range correlations in rapidity and thus are not directly connected with the overall geometry of the initial state of the collision. Comparison of these data with AMPT results [11] shows that the model gives the same qualitative trend as the data in the same η acceptance, but with K_{eff} values systematically lower by about 0.4. Note that the values of K_{eff} and δ are extracted in a limited acceptance of $|\eta| < 3$ and, therefore, are normally smaller than for a full acceptance measurement. The acceptance effect is discussed quantitatively in the next section. In AMPT at the generator level, the decrease in effective cluster size with increasing event centrality appears to be related to the hadronic rescattering stage. Turning off hadronic rescattering processes in AMPT leads to a larger effective cluster size in both Au + Au and Cu + Cu that is approximately invariant for all centralities.

Further detailed studies on cluster properties have also been performed. The entire analysis was repeated for pairs in the restricted $\Delta\phi$ range. Instead of averaging over the whole $\Delta\phi$ region, the cluster parameters can be extracted for pairs in the near-side and away-side $\Delta\phi$ ranges ($0° < \Delta\phi < 90°$ and $90° < \Delta\phi < 180°$, respectively). Clusters with high p_T generally contribute more pairs on the near side, whereas away-side pairs mainly come from lower-p_T clusters. In this restricted averaging, the $\cos(2\Delta\phi)$ elliptic flow component again averages to zero. The results are shown in Fig. 5 as a function of fractional cross section for Cu + Cu and Au + Au collisions at $\sqrt{s_{NN}} = 200$ GeV. The overall scale error is 3% for the near-side data and 5% for the away-side data, for both K_{eff} and δ. Over the studied centrality range, the effective cluster size extracted for pairs from the away side decreases by about 30%–40% with increasing centrality, whereas the decrease for the near side is somewhat smaller. This behavior could be understood in a scenario where the medium is extremely dense at more central collisions and only clusters produced close to the surface can survive. Then for low-p_T clusters, it
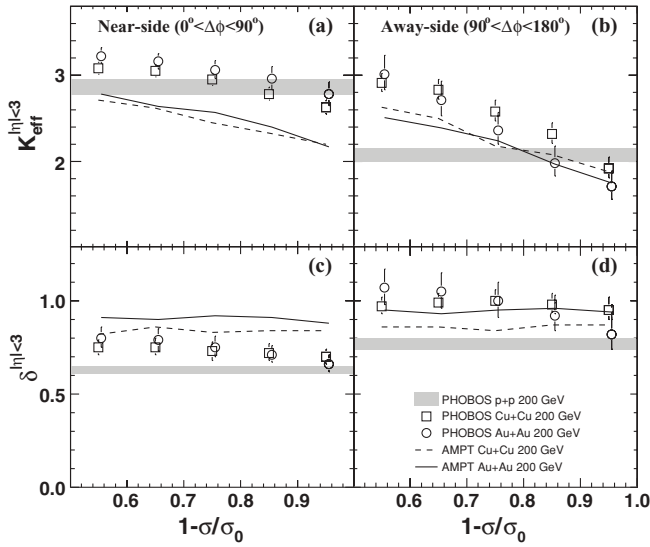
FIG. 5. Near-side and away-side K_{eff} (a and b) and δ (c and d) as a function of fractional cross section $[1 - (\sigma/\sigma_0) = 1$ for the most central collisions], for PHOBOS data (open symbols) and for the AMPT model (lines), in $Cu + Cu$ (squares) and $Au + Au$ (circles) collisions for $|\eta| < 3$ at $\sqrt{s_{NN}} = 200$ GeV. Error bars for data points represent systematic errors with 90% confidence limits. Results for $p + p$ collisions at $\sqrt{s} = 200$ GeV [6] are shown by the shaded band.

is more likely that a portion of the decay particles travels into the medium and gets absorbed, resulting in a suppression of away-side correlations. As for the observed collision geometry scaling of the effective cluster size, it might be related to the surface-to-volume ratio of the system. More detailed modeling is still being investigated to understand these phenomena. In this case, AMPT shows a smaller difference in cluster properties between the near and the away side than observed in the data.

V. CORRECTING FOR LIMITED ACCEPTANCE

As mentioned in the previous section, some particles from cluster decay fall outside of the PHOBOS Octagon detector acceptance in pseudorapidity ($|\eta| < 3$). This reduces both K_{eff} and δ. To quantitatively study this effect, a simple ICM as well as several dynamical models are used. In our ICM approach, for each event clusters are generated, each with a given mass, transverse momentum, p_T, and η. The cluster

decays isotropically in its rest frame into K particles (assumed to be pions) constrained by the available phase space. The mass of the clusters is taken to be $0.35 \times K$ (GeV/c^2). The p_T and η of the clusters are drawn from distributions that have been tuned such that the final inclusive charged particles match the measured spectra [12–14]. In addition, the global momentum of the clusters is always conserved event by event to preserve the $\cos(\Delta\phi)$ component typically seen in the $p + p$ 2D correlation function (e.g., in Fig. 2(a)).

In Fig. 6(a), an example of a 2D two-particle correlation function from ICM is shown with $K = 3$ measured in an acceptance of $|\eta| < 3$. It shows a structure qualitatively similar to that observed in $p + p$ collisions in Fig. 2(a): a Gaussian-shape short-range correlation along $\Delta\eta$ that gets wider going from near side to away side. The narrow peak in the near-side part of the correlation function is primarily from higher-p_T clusters as well as three-body decays (e.g., in Ref. [3]), whereas the broader away side generally arises from the decay of clusters with a lower p_T. Figure 6(b) shows a comparison of 1D $\Delta\eta$ correlation functions measured in the limited acceptance of $|\eta| < 3$ versus the full acceptance. From this comparison, one can see that the shape is significantly modified by the limited acceptance, resulting in reductions in both K_{eff} and δ. By comparing the cluster parameters extracted for the acceptance of $|\eta| < 3$, $K_{eff}^{|\eta|<3}$ and $\delta^{|\eta|<3}$, with those extracted for the full acceptance, $K_{eff}^{|\eta|<\infty}$ and $\delta^{|\eta|<\infty}$, an acceptance correction can be obtained in the context of the ICM.

Note that in the ICM, δ is not an independent variable but, rather, depends on the cluster p_T for a given cluster mass. The higher the p_T is, the narrower the cluster width will be. In a scenario of isotropic decay of the clusters, the maximum possible width turns out to correspond to $\delta^{|\eta|<3} \sim 0.75$ for $K = 2$ and the p_T of all clusters fixed at 0, which is lower than the cluster width observed in $A + A$ collisions (~ 0.9 in the most peripheral collisions). Therefore, to generate a wider range of possible δ parameter values in the ICM, another parameter, γ, is introduced to artificially modify the width of the clusters by rescaling the relative pseudorapidity of each decay product:

$$\eta_i' - \eta_0 = \gamma \times (\eta_i - \eta_0), \quad i = 1, 2, 3, \ldots, \quad (7)$$

where η_0 represents the pseudorapidity of the original clusters, and η_i and η_i' correspond to the pseudorapidity of decaying particles from clusters before and after modification. In this way, any value of the cluster width can be obtained while
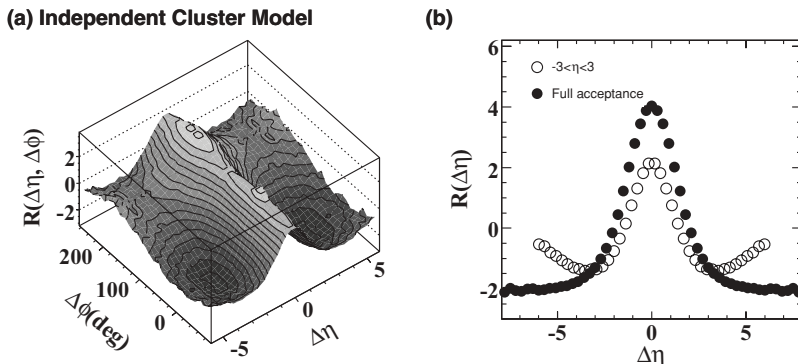

(a) Independent Cluster Model

(b)

FIG. 6. (a) 2D two-particle correlation function in $\Delta\eta$ and $\Delta\phi$ for ICM with $K = 3$ and $\gamma = 0$ [defined in Eq. (7)]. (b) Comparison of 1D pseudorapidity correlation function for the ICM with $K = 3$ and $\gamma = 0$ [defined in Eq. (7)] between the acceptance of $|\eta| < 3$ and the full acceptance.
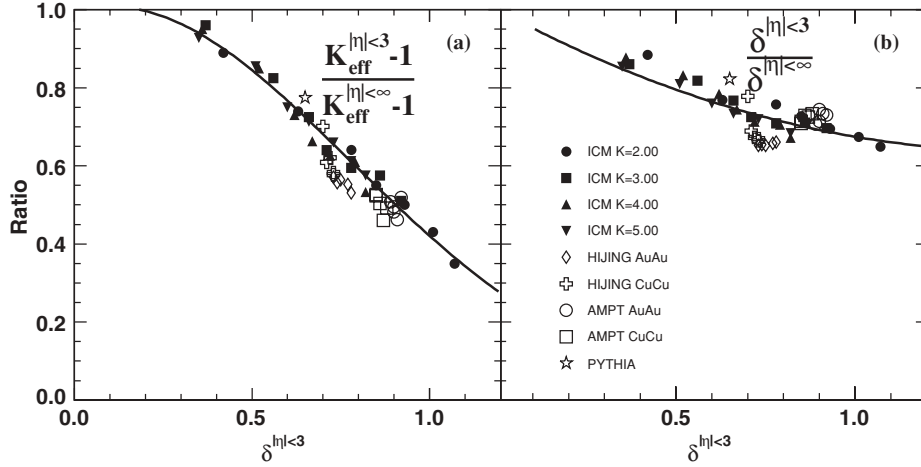
FIG. 7. Ratio of (a) $K_{\mathrm{eff}}^{|\eta|<3} - 1$ to $K_{\mathrm{eff}}^{|\eta|\langle\infty} - 1$ and (b) $\delta^{|\eta|<3}$ to $\delta^{|\eta|\langle\infty}$ as a function of $\delta^{|\eta|\langle 3}$ obtained in the ICM (filled symbols) as well as the PYTHIA, HIJING, and AMPT models (open symbols). The solid line is a smooth function fit to all the models.

keeping the original η of the cluster unchanged. For each set of K and γ, the $dN/d\eta$ and dN/dp_T distributions of the clusters are tuned to match those of the final-state inclusive charged particles measured in the data.

The ICM, with a range of values of K and γ, has been used to generate a set of two-particle correlation functions, for both $|\eta| < 3$ and the full acceptance. In Fig. 7, the ratios $(K_{\mathrm{eff}}^{|\eta|<3} - 1)/(K_{\mathrm{eff}}^{|\eta|<\infty} - 1)$ and $\delta^{|\eta|<3}/\delta^{|\eta|<\infty}$ from the ICM are shown as a function of $\delta^{|\eta|<3}$, as extracted directly from fits to the correlation function. It is clearly seen that the suppression of these ratios are primarily a function of $\delta^{|\eta|<3}$ only, and both K_{eff} and δ are suppressed more as $\delta^{|\eta|<3}$ increases. This is because correlated particles are more likely to fall outside the measured region as the cluster width increases. The suppression factors in dynamical models like PYTHIA [15] for $p + p$, HIJING [16], and AMPT for $Cu + Cu$ and $Au + Au$ at various centralities are also calculated. All models are consistent within about 5%–10%. A second-order polynomial function is fitted to the values of all models to generate a smooth correction function. This function is applied to the measured $K_{\mathrm{eff}}^{|\eta|<3}$ and $\delta^{|\eta|<3}$ using Eq. (9) to estimate $K_{\mathrm{eff}}^{|\eta|<\infty}$ and $\delta^{|\eta|<\infty}$ for the experimental data:

$$\left(K_{\mathrm{eff}}^{|\eta|<\infty} - 1\right)_{\mathrm{data}} = \frac{\left(K_{\mathrm{eff}}^{|\eta|<\infty} - 1\right)_{\mathrm{MC}}}{\left(K_{\mathrm{eff}}^{|\eta|<3} - 1\right)_{\mathrm{MC}}} \times \left(K_{\mathrm{eff}}^{|\eta|<3} - 1\right)_{\mathrm{data}},$$

$$\delta_{\mathrm{data}}^{|\eta|<\infty} = \frac{\delta_{\mathrm{MC}}^{|\eta|<\infty}}{\delta_{\mathrm{MC}}^{|\eta|<3}} \times \delta_{\mathrm{data}}^{|\eta|<3}. \tag{8}$$

The scattering of the points around the fitted correction curves in Fig. 7 is taken into account as one source of the systematic uncertainties on the acceptance correction procedure. As a cross-check, the cluster parameters in the data have also been measured in $|\eta| < 2$. The ratios, $(K_{\mathrm{eff}}^{|\eta|<2} - 1)/(K_{\mathrm{eff}}^{|\eta|<3} - 1)$ and $\delta^{|\eta|<2}/\delta^{|\eta|<3}$, are found to be consistent with the ICM and dynamical models. The residual discrepancies between the results extrapolated to full phase space from $|\eta| < 2$ and $|\eta| < 3$ are used to estimate a separate contribution to the systematic uncertainty of the acceptance correction. The total uncertainty of the correction is thus found to be 12% for K_{eff} and 9% for δ.

After applying the acceptance correction, the cluster parameters at full phase space, $K_{\mathrm{eff}}^{|\eta|<\infty}$, and $\delta^{|\eta|<\infty}$, in $p + p$, $Cu +$

Cu, and $Au + Au$ collisions at $\sqrt{s_{NN}} = 200$ GeV, are shown in Fig. 8 for the inclusive (left column), near-side (middle column), and away-side (right column) K_{eff} and δ along with the results from AMPT. The systematic errors come not only from the measurement itself but also from the acceptance correction procedure. The values of K_{eff} and δ in $p + p$ collisions extrapolated to full phase space are larger than those presented in Ref. [6], measured in a limited acceptance of $|\eta| < 3$, and better reflect the properties of the clusters produced in these reactions. Because δ measured in both $Cu + Cu$ and $Au + Au$ collisions at PHOBOS only weakly depends on centrality, the geometric scaling feature of K_{eff} between the two systems still holds after the acceptance correction as shown in Fig. 8. That said, the large values of $K_{\mathrm{eff}}^{|\eta|<\infty}$ and $\delta^{|\eta|<\infty}$ clearly pose a challenging question as to the origin of such strong correlations with such a long range. In calculations from the Therminator model that include all known resonances [17], K_{eff} is approximately 2 and δ is no larger than 0.75, whereas in peripheral $A + A$ collisions, there appear to be clusters that decay into five or six charged particles with much larger δ. This was not something expected from previous data on $p + p$ collisions, although there are data on $\langle p_T \rangle$ fluctuations from STAR [18] and PHENIX [19] that have been interpreted as evidence for similarly large clusters in $Au + Au$ collisions [20]. The production of jets is a natural mechanism to induce clustering phenomena, although one would expect jets to lead to a smaller δ than isotropic decay. It is also possible that additional correlation sources, such as dynamical fluctuation of the $dN/d\eta$ distribution event by event, may modify the two-particle correlations in a way that leads to an increase in the observed effective cluster size. The fact that $\delta^{|\eta|<\infty}$ in peripheral $A + A$ collisions is larger than $p + p$, and far exceeds the value expected for isotropic decay, also begs the question of how the cluster decays are "elongated" in phase space. Finally, it is observed that cluster parameters in central events approach values measured in $p + p$ collisions, whereas those in peripheral events are substantially higher—almost a factor of 2 in terms of $K_{\mathrm{eff}} - 1$ (which is equivalent to the so-called "conditional yield" in analyses involving high-p_T-triggered hadrons). Overall, more theoretical insights are needed to understand these surprising features of two-particle correlations in heavy ion collisions.
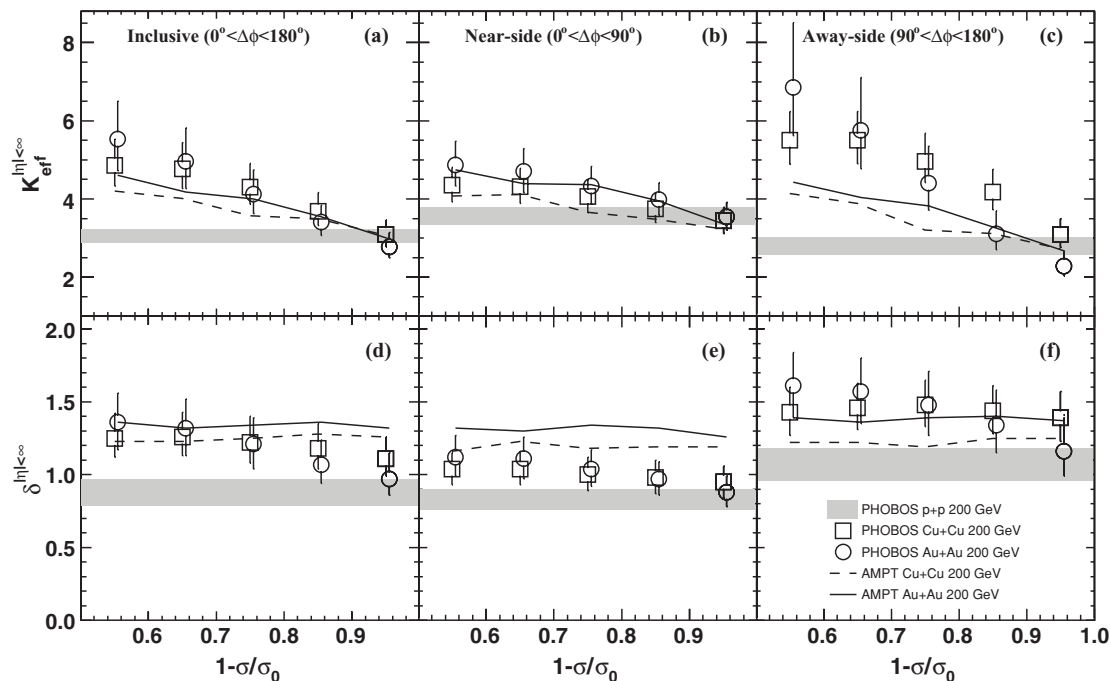
FIG. 8. Inclusive, near-side, and away-side K_{eff} (a, b, and c) and δ (d, e, and f) as a function of fractional cross section [$1 - (\sigma/\sigma_0) = 1$ for the most central collisions] measured by PHOBOS (open symbols) and from the AMPT model (lines) after correction to the full acceptance in Cu + Cu (squares) and Au + Au (circles) collisions at $\sqrt{s_{NN}} = 200$ GeV. Error bars for data points represent systematic errors with 90% confidence limits. Results for $p + p$ collisions at $\sqrt{s} = 200$ GeV after correction to the full acceptance are shown in the shaded band, which are larger than those in Ref. [6] measured in an acceptance of $|\eta| < 3$.

VI. SUMMARY AND CONCLUSION

The two-particle correlation function for inclusive charged particles has been extensively studied over a broad range of $\Delta\eta$ and $\Delta\phi$ in $p + p$, Cu + Cu, and Au + Au collisions at $\sqrt{s_{NN}} = 200$ GeV. In particular, it has been shown that the correlation functions in heavy ion collisions are not very different from those found in $p + p$, allowing a similar interpretation in terms of clusters. In this approach, multiple particles are understood to be emitted close together in phase space, with a typical effective cluster size of 2.5–3.5 charged particles in $p + p$ collisions. The correlation functions in $A + A$ show a nontrivial decrease in effective cluster size with increasing centrality and a surprising geometric scaling between Cu + Cu and Au + Au collisions. Analysis of near- and away-side clusters provides additional information on the details of the cluster properties. Extrapolating the measured cluster parameters to the full phase space using an independent cluster model as well as other dynamical models such as PYTHIA, HIJING, and AMPT, the effective cluster size and width increase in magnitude to a level that seems to challenge most conventional scenarios of the hadronization process. Clearly, more experimental and theoretical work will be needed to understand these novel aspects of heavy ion collisions.

[1] R. E. Ansorge *et al.* (UA5 Collaboration), Z. Phys. Particle Fields C **37**, 191 (1988).

[2] F. Henyey, Phys. Lett. **B45**, 469 (1973); E. L. Berger, Nucl. Phys. **B85**, 61 (1975); J. L. Meunier and G. Plaut, *ibid.* **B87**, 74 (1975); C. Michael, *ibid.* **B103**, 296 (1976).

[3] K. Eggert *et al.*, Nucl. Phys. **B86**, 201 (1975).

[4] D. Drijard *et al.*, Nucl. Phys. **B155**, 269 (1979).

[5] A. Morel and G. Plaut, Nucl. Phys. **B78**, 541 (1974).

[6] B. Alver *et al.*, Phys. Rev. C **75**, 054913 (2007).

[7] L. J. Shi and S. Jeon, Phys. Rev. C **72**, 034904 (2005).

[8] B. B. Back *et al.*, Nucl. Instrum. Methods A **499**, 603 (2003).

[9] B. B. Back *et al.*, Phys. Rev. Lett. **87**, 102303 (2001); P. Sarin, Ph.D. thesis, Massachusetts Institute of Technology, 2003; W. Li, Ph.D. thesis, Massachusetts Institute of Technology, 2009.

[10] N. Borghini, P. M. Dinh, and J.-Y. Ollitrault, Phys. Rev. C **63**, 054906 (2001).

[11] Z. W. Lin, C. M. Ko, B. A. Li, B. Zhang, and S. Pal, Phys. Rev. C **72**, 064901 (2005).

[12] B. B. Back *et al.*, Phys. Rev. Lett. **91**, 052303 (2003).

[13] B. Alver *et al.*, arXiv:0709.4008v1 (2007).

[14] S. Adler *et al.*, Phys. Rev. C **69**, 034909 (2004).

[15] T. Sjostrand, S. Mrenna, and P. Skands, J. High Energy Phys. 05 (2006) 026 [Version 6.325, single diffractive process excluded].

[16] M. Gyulassy and X. N. Wang, Comput. Phys. Commun. **B83**, 307 (1994) [Version 1.383, single diffractive process excluded].

[17] A. Kisiel, T. Taluc, W. Broniowski, and W. Florkowski, Comput. Phys. Commun. **174**, 669 (2006) [arXiv:nucl-th/0504047]; Calculation by A. Kisiel (private communication).

[18] J. Adams *et al.*, Phys. Rev. C **71**, 064906 (2005); **72**, 044902 (2005).

[19] K. Adcox *et al.*, Phys. Rev. C **66**, 024901 (2002); S. S. Adler *et al.*, Phys. Rev. Lett. **93**, 092301 (2004).

[20] W. Broniowski, P. Bozek, W. Florkowski, and B. Hiller, PoS **CFRNC2006**, 020 (2006) [arXiv:nucl-th/0611069].